Proc. Natl. Acad. Sci. USA
Vol. 81, pp. 7941–7945, December 1984
Medical Sciences

Microtubule-associated protein 2: Monoclonal antibodies demonstrate the selective incorporation of certain epitopes into Alzheimer neurofibrillary tangles

(Alzheimer disease/paired helical filaments/dendrites/phosphorylation)

KENNETH S. KOSIK*†, LAWRENCE K. DUFFY*†, MICHAEL M. DOWLING*, CARMELA ABRAHAM*, ALAN MCCLUSKEY*, AND DENNIS J. SELKOE*†

*Ralph Lowell Laboratories, Mailman Research Center, McLean Hospital, Belmont, MA 02178; and †Department of Neurology, Harvard Medical School, Boston, MA 02115

Communicated by Walle J. H. Nauta, August 24, 1984

ABSTRACT **Neurofibrillary tangles (NFT) are the principal structural alteration of neuronal cell bodies in Alzheimer disease as well as in normal aging of the human brain. While the ultrastructure of these intraneuronal lesions has been extensively studied, the biochemical composition of the fibers comprising the NFT is unknown. We report the production of three monoclonal antibodies against the microtubule-associated protein 2 (MAP-2), one of which intensely labels Alzheimer NFT. All three antibodies specifically recognize MAP-2 on immunoblots and stain brain tissue in a characteristic dendritic pattern. The three antibodies are directed against at least two different antigenic sites on the MAP-2 molecule, and one appears to recognize a phosphorylation site on MAP-2. That only one of the three antibodies immunolabels NFT suggests that the formation of the tangle involves some modification of the MAP-2 molecule. Our findings suggest that one aspect of Alzheimer-type neurofibrillary pathology is an aggregation of MAP-2 or MAP-2 fragments with altered neurofilamentous elements present in NFT. Normal interactive function, which putatively occurs between neurofilaments and MAP-2, may thus be disrupted in Alzheimer disease.**

The neurofibrillary tangle (NFT) is one of the major neuronal structural changes that characterize Alzheimer disease, but it also occurs during normal aging of the brain. By electron microscopy, the NFT is composed almost entirely of paired helical filaments (PHF) (20–22 nm, maximal diameter), intermixed with some straight filaments (1–4). These straight filaments range in diameter from 10 nm (the dimension of normal neurofilaments) to 15 nm (5–11). The PHF differ from normal neurofilaments in their marked insolubility (12), the apparent absence of certain neurofilament antigenic determinants in their structure (13, 14), the presence of some unique determinants (15), and the slightly larger diameter of each member filament than normal neurofilaments (4–7, 9–11). The protein composition of the PHF remains unknown because their insolubility prevents the application of most analytical techniques. While the chemical composition of PHF has not been ascertained, it appears that some normal fibrous proteins or protein fragments are found within the NFT. Neurofilaments are likely to be among such proteins (13, 16–20). We report here the raising of monoclonal antibodies (mAb) to microtubule-associated protein 2 (MAP-2) and the finding that certain MAP-2 epitopes are associated with Alzheimer NFT, both *in situ* and after isolation of the tangles under nondenaturing conditions.

MAP-2, a M_r ≈300,000 protein, copurifies with tubulin and several other proteins when microtubule-enriched fractions are prepared by temperature-dependent phases of assembly and disassembly (21). Under certain buffer conditions, MAP-2 stimulates the assembly of pure tubulin (22–24). Using various ultrastructural techniques, MAP-2 molecules appear as projections extending outward from the microtubule wall (22, 24–26). Unlike some of the other MAPs, MAP-2 is highly concentrated in neuronal dendrites and soma, while axons and non-neuronal elements appear free of the antigen when brain tissue sections are examined immunohistochemically (27, 28). Because of the putative role of MAP-2 in providing a site of interaction between microtubules and neurofilaments (29–37), and because Alzheimer-type neuronal degeneration involves a reorganization of the cytoskeleton, we hypothesized that MAP-2 might play a role in this complex reorganization.

METHODS

Rat brain microtubules were purified through two cycles of polymerization/depolymerization according to the method of Shelanski *et al.* (38) and were used as an immunogen in mice. An electrophoretogram of this material is shown in Fig. 1. One milligram of the preparation was emulsified in complete Freund's adjuvant. Half of this material was injected intraperitoneally and half was injected at several subcutaneous sites in a 5-wk-old female BALB/c mouse. Two additional injections with 500 μg of the preparation emulsified in incomplete Freund's adjuvant were given in a similar fashion at 4 and 6 wk after the initial immunization. Eight weeks after the initial immunization, the mouse was sacrificed and its spleen was excised. Spleen cells (2×10^8) were fused to 1.7×10^7 logarithmic phase NS1 mouse myeloma cells in 50% (wt/vol) polyethylene glycol 1540 using the method of Kennett (39). Three weeks after fusion, samples of the cell supernatants were screened for the production of specific antibody by an ELISA (40) in which a 0.2- to 2.0-μg sample of the antigen was bound to Microtest III Flexible Assay Plates (Falcon). Clones that reacted positively by ELISA were analyzed by the immunoblot procedure of Towbin *et al.* (41) using the microtubule preparation as the substrate. Tubulin and MAPs prepared either by the method of Shelanski *et al.* (38) or by the taxol method of Vallee (42) were electrophoresed (43) and transferred to nitrocellulose paper (41). This material was immunostained with the supernatants from those clones that reacted strongly with the microtubule preparation by ELISA. Positive clones by immunoblot (of which there were three) were subcloned twice in Dulbecco's modified Eagle's medium with 20% heat-inactivated fetal bovine serum (HyBRL Prep, Bethesda Research Laboratories)

The publication costs of this article were defrayed in part by page charge payment. This article must therefore be hereby marked "*advertisement*" in accordance with 18 U.S.C. §1734 solely to indicate this fact.

Abbreviations: NFT, neurofibrillary tangles; MAP, microtubule-associated protein; PHF, paired helical filaments; mAb, monoclonal antibodies.

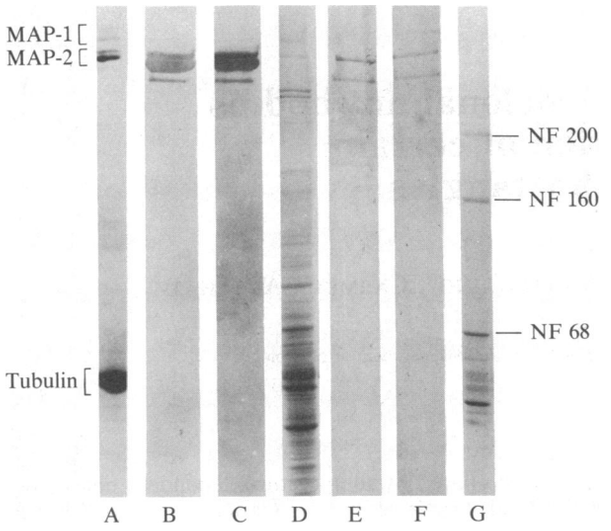

FIG. 1. Lane A, Coomassie brilliant blue-stained microtubular preparation (30 μg) used as the mouse immunogen (see *Methods*). Lane B, immunoblot of microtubular preparation stained with 5F9. Lane C, immunoblot of microtubular preparation stained with 4F7. Both 5F9 and 4F7 are specific for the MAP-2 bands. Lane D, Coomassie brilliant blue-stained total homogenate of rat forebrain. Lane E, immunoblot of rat forebrain homogenate stained with 5F9. Lane F, immunoblot of rat forebrain homogenate stained with 4F7. Lane G, Coomassie brilliant blue-stained neurofilament preparation. Components of the triplet are indicated by the designation NF followed by the $M_r \times 10^{-3}$.

by the limited dilution technique (44). Antibody-producing hybrids were grown in medium, or as ascites tumors in Pristane-primed BALB/c mice. Antibody produced in tissue culture was precipitated with ammonium sulfate and concentrated 5-fold before storage at −70°C.

Demonstration of mAb immunoreactivity directed against a phosphate-containing site was done by the method of Sternberger and Sternberger (45). Nitrocellulose sheets upon which a microtubule preparation had been transferred were incubated in bovine intestinal alkaline phosphatase (type VII, Sigma). Because the enzyme may not be pure, nitrocellulose sheets were also incubated in alkaline phosphatase with 50 mM phosphate (46), which served to inhibit the reaction and ensure that altered MAP-2 immunoreactivity was due to the alkaline phosphatase. NFT were analyzed for their immunoreactivity in three forms:

(*i*) Sections (10 μm) from formalin-fixed paraffin-embedded Alzheimer brain tissue were used to determine the immunoreactivity of NFT *in situ*.

(*ii*) Isolated NFT prepared under non-denaturing conditions in a physiologic buffer (15, 17) were immunostained. Five to 10 g from NFT-rich areas of frozen Alzheimer disease cerebral cortex were homogenized in 10 vol of Tris saline buffer (50 mM Tris·HCl, pH 7.6/145 mM NaCl). The homogenate was sieved through a 200-μm nylon mesh and centrifuged at 100,000 × *g* for 30 min at 4°C. The pellet was rehomogenized in Tris saline buffer and was layered on top of 1 M sucrose in Tris saline and spun at 100,000 × *g* for 45 min. The resultant pellet was resuspended in 100 μl of Tris saline buffer, and 2-μl aliquots of these NFT-enriched fractions were placed on albumin-coated slides, air dried, and immunostained.

(*iii*) Isolated NFT prepared under denaturing conditions in $NaDodSO_4$ and 2-mercaptoethanol (15, 17) were also immunostained. For this purpose, NFT-rich frozen Alzheimer cerebral cortex was minced and incubated in 10 vol of 2% $NaDodSO_4$ buffer (50 mM Tris·HCl, pH 7.6/2% (wt/vol) $NaDodSO_4$/0.1 M 2-mercaptoethanol) for 2 hr at room temperature. This suspension was homogenized, heated to 100°C for 5 min, sieved, and the filtrate was spun at 100,000 × *g* for 30 min at 25°C. The resultant pellet was suspended in 1% $NaDodSO_4$ buffer and homogenized. One-milliliter aliquots of this suspension were layered on top of a sucrose gradient containing 2.0 M and 1.5 M sucrose in $NaDodSO_4$ buffer and spun at 243,000 × *g* for 2 hr at 25°C. Material at the 1.5/2.0 M interface was collected and spun at 100,000 × *g* for 60 min.

Electron microscopy of this final pellet revealed abundant masses of PHF as well as isolated PHF. The dimensions and helical periodicity of these fibers were similar to those of PHF *in situ*. Other $NaDodSO_4$-insoluble material seen in the pellet included lipofuscin granules and amyloid cores of senile plaques. Two-microliter aliquots of these NFT-enriched fractions were placed on albumin-coated slides for immunostaining.

Tangles isolated in either Tris saline or $NaDodSO_4$ buffers could be recognized as Alzheimer NFT by their characteristic shapes, fibrous appearance, and green birefringence under polarized light after Congo red staining. NFT were immunostained with the primary antibodies followed by goat anti-mouse peroxidase-conjugated IgG (Cappel Laboratories, Cochranville, PA) (1:100). Immunohistochemistry was assayed on both formalin-fixed human brain sections and perfused rat brain using the indirect peroxidase technique (47).

RESULTS

Approximately one-third of the primary clones established after the fusion showed some immunoreactivity with the microtubule preparation by ELISA. The six strongest reacting clones were analyzed on immunoblots, and three of these six showed reactivity with proteins in the twice-cycled microtubule preparation. All three clones, referred to as 5F9, 4F7, and 4D5, appeared to react specifically with MAP-2 (Fig. 2). There was no cross-reactivity with any proteins in a neurofilament preparation (data not shown), and the few immunoreactive protein species just below MAP-2 in total rat brain homogenates (Fig. 1) were thought to represent MAP-2 proteolytic products.

A more detailed analysis of the precise immunoreactive patterns of each antibody on taxol-prepared MAP-2 from rat brain was performed using high resolution $NaDodSO_4$/polyacrylamide gel electrophoresis and immunoblotting. In Coo-

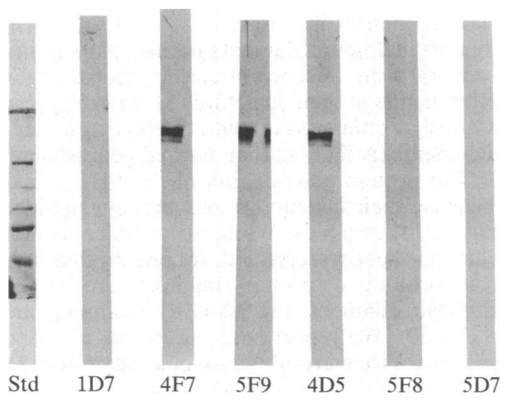

FIG. 2. Gel blots of the microtubular preparation using supernatants from the six clones that were most reactive by ELISA. The number of each clone is designated. Three of the clones are immunoreactive with proteins in the region of MAP-2. Clones with no immunoreactivity on the gel blots may produce an antibody that does not recognize the protein in the $NaDodSO_4$-containing electrophoretic buffers. $M_r \times 10^{-3}$ standards (Std) (top to bottom) are 200, 116, 92, 66, 45, and 31.

massie-stained gels, we observed a protein doublet of M_r ≈300,000 considered to represent MAP-2 (Fig. 1). A third weaker MAP-2 immunoreactive band was present just below the doublet (Fig. 1). The MAP-1 protein bands of M_r ≈350,000 are also indicated in Fig. 1. Even with silver staining, no further detail could be detected in this region. One-dimensional peptide maps (48) of each component of the MAP-2 doublet using *Staphylococcus aureus* V8 protease were identical (data not shown). All three proteins in the region of MAP-2 were immunostained by each of the three mAbs, whereas the MAP-1 bands did not react (Fig. 1). Each of the MAP-1 bands and each of the three MAP-2 bands was individually cut from the gel and re-electrophoresed. Again, neither of the MAP-1 bands stained with the mAb, and all three of the MAP-2 bands were immunoreactive (data not shown). Whether these three forms of MAP-2 with slightly different electrophoretic mobilities represent native heterogeneity of the molecule or are proteolytic products related to isolation is unknown.

MAP-2 is known to be highly sensitive to proteolysis, and this property was used to generate multiple proteolytic fragments in an attempt to distinguish the three mAbs by different immunoreactive patterns. A twice-cycled microtubule preparation was repeatedly frozen and thawed to generate a ladder of proteolytic fragments beneath MAP-2 on NaDodSO$_4$/acrylamide gels. These gels were then immunoblotted with each of the three mAbs (Fig. 3). Most of the proteolytic fragments were stained by all three antibodies, and the patterns produced by 4F7 and 4D5 were identical. 5F9, however, failed to stain certain high M_r fragments, suggesting that this antibody recognizes a different epitope than do 4F7 and 4D5. The pattern of MAP-2 immunoreactive proteolytic products was highly reproducible.

The mAbs were also compared with regard to their ability to distinguish functional states of MAP-2 dependent on phosphorylation (45). Treatment of electroblots with alkaline phosphatase markedly reduced the intensity of MAP-2 immunostaining with 4F7, but not with 5F9 (Fig. 4). Staining was not, however, completely abolished even when the concentration of alkaline phosphatase was doubled to 86 μg/ml or when incubation at 32°C was lengthened to 15 hr. The marked reduction in immunoreactivity after alkaline phosphatase treatment could not be duplicated using acid phosphatase (potatoe, type III, Sigma). The effect of alkaline phosphatase could be completely inhibited by 50 mM phosphate added to the incubation buffer (0.1 M Tris·HCl, pH 8.0/0.01 M phenylmethylsulfonyl fluoride/43 μg of alkaline phosphatase).

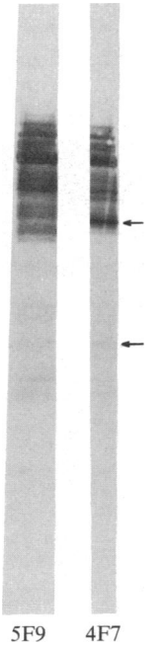

FIG. 3. Gel blot of a repeatedly frozen and thawed microtubular preparation. Under these conditions, MAP-2 forms a ladder of proteolytic fragments in the $M_r \times 10^{-3}$ range of 280 to 150. Fragments were immunostained with the anti-MAP-2 mAbs 5F9 and 4F7. Arrows indicate MAP-2 fragments recognized only by 4F7.

FIG. 4. Immunoblot of microtubular preparation stained with 4F7. Before incubation with primary antibody, the nitrocellulose strips were incubated in buffer with (lane B) and without (lane A) alkaline phosphatase. Phosphatase treatment results in a marked reduction in immunoreactivity of the MAP-2 bands.

Because MAP-2 is preferentially distributed in dendrites (27), we analyzed rat brain immunohistochemically to determine whether our antibodies produce a dendritic staining pattern. Fig. 5 shows a paraffin section of perfused rat cerebral cortex, demonstrating deposition of antibody (5F9) in the apical shafts of pyramidal cell dendrites and within the perikaryon. The antigen could not be detected in glial cells. White matter tracts (i.e., axons) in the centrum semiovale, cerebellum, and spinal cord do not stain; however, dendritic arbors do extend into the white matter. Dendritic staining is also apparent in rabbit, mouse (49), and human brain tissue; however, human tissue shows a reduced staining intensity, probably because of postmortem and fixation factors. The antigen is definitely present in human tissue because immunoreactivity in the MAP-2 region can readily be demonstrated on gel blots of human brain tissue (data not shown).

The immunostaining properties of NFT were studied with

FIG. 5. Dendritic pattern of anti-MAP-2 immunoreactivity. Coronal section of 6-month-old rat cerebral cortex immunostained with 5F9 followed by peroxidase-conjugated goat anti-mouse IgG and visualized with 3,3′-diaminobenzidine tetrahydrochloride. Apical shafts of pyramidal cell dendrites stain most prominently. (×225.)

the MAP-2 mAb in three brains from patients with Alzheimer disease and one brain from a patient with Down syndrome and Alzheimer disease (50–52). Formalin-fixed hippocampal sections containing numerous NFT were immunoreacted with 5F9 and 4F7. Only 5F9 immunostained the NFT (Fig. 6). NFT were isolated from cerebral cortex under nondenaturing conditions (Tris saline; see *Methods*) and again only 5F9 produced immunoreactivity (Fig. 7). The mAbs 4F7 and 4D5 did not label NFT either *in situ* or after isolation. When NFT were isolated under denaturing conditions—i.e., by heating in $NaDodSO_4$ and 2-mercaptoethanol—all immunoreactivity of the tangles with the 5F9 antibody was lost.

In Alzheimer brain tissue sections, 5F9 produced particularly intense staining of so-called "ghost" tangles (Fig. 8). This term is used to refer to NFT that by light microscopy are no longer associated with a nucleus and appear to have lost their surrounding neuronal structure (17). The individual fibrils of the "ghost" tangle, rather than appearing densely compacted as they do intraneuronally, display a more open, loose appearance. They are typically found in areas of brain of Alzheimer disease patients that tend to be intensely affected, such as CA1 of the hippocampus and the parahippocampal cortex. Neither the amyloid cores nor the abnormal neurites comprising senile plaques were stained by 5F9.

DISCUSSION

The biochemical composition of the fibrous elements comprising NFT is currently unknown. Immunocytochemical evidence to date indicates that NFT are complex in their protein composition and include some antigens that cross-react with normal cytoskeletal proteins. Immunolabeling with mAb has served to identify certain determinants that NFT share with cytoskeletal proteins. Antigens from the neurofilamentous system have been found in NFT (13, 16), and we now report that at least one antigen from the microtubular system is also present in NFT on the basis of immunocytochemical criteria. Anderton *et al.* (13) have reported two mAbs, called RT97 and BF10, that label NFT *in situ* and specifically react with the M_r 200,000 and M_r 160,000 neurofilament proteins, respectively. Autilio-Gambetti *et al.* have described similar mAbs to the high M_r neurofilament proteins that immunolabel NFT (16). Reports of antibodies to microtubular preparations that immunoreact with NFT have not characterized the specificity of the antibody with regard to individual microtubule or microtubule-associated proteins (53, 54). In the work reported here, we demonstrate that NFT from brains with Alzheimer disease and Alzheimer disease associated with Down syndrome share at least one antigenic determinant with the MAP-2 molecule. The mAb against MAP-2, 5F9, recognizes a determinant present in

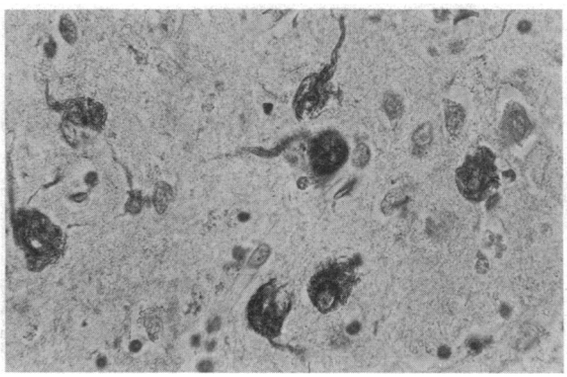

FIG. 6. NFT within neuronal cell bodies labeled with mAb 5F9 to MAP-2. Paraffin sections of formalin-fixed Alzheimer disease hippocampal cortex stained by the peroxidase-conjugated secondary-antibody method. (×225.)

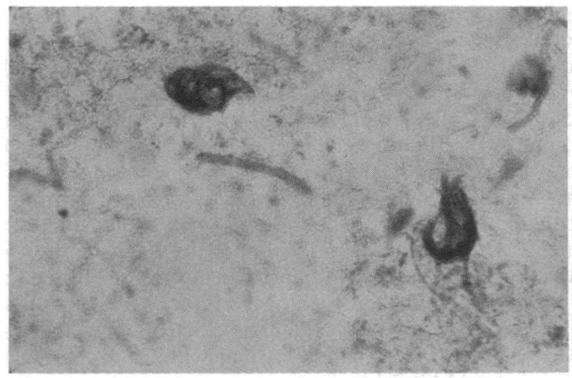

FIG. 7. NFT isolated by Tris saline method and labeled with mAb 5F9 to MAP-2. A suspension of isolated NFT is pipetted onto an albumin-coated slide and stained by the peroxidase-conjugated secondary-antibody method. (×450.)

NFT; however, 4F7 and 4D5, which are directed against other determinants of MAP-2 (Fig. 3), do not immunolabel NFT. The formation of NFT, therefore, appears to involve some modification of the MAP-2 molecule, because the epitope(s) recognized by 4F7 and 4D5 either are lost or are not exposed, while the 5F9 epitope is retained and exposed. The modification may occur at a phosphorylation site, since 4F7, which does not recognize NFT, also loses its immunoreactivity with MAP-2 after alkaline phosphatase treatment. The loss of immunoreactivity was attributed to phosphatase treatment rather than to a contaminant in the enzyme preparation, because it could be completely inhibited by 50 mM phosphate. Failure to obtain complete eradication of staining after phosphatase treatment might be because the antibody still recognizes the same site on the protein even without the phosphate; however, it has a reduced affinity with the dephosphorylated form. Alternatively, the phosphatase may not remove phosphates from all the MAP-2 molecules in the nitrocellulose sheet.

Recently, a polyclonal antiserum to MAP-2 has been shown to stain abnormal neurites around senile plaques (55). This antiserum stained perikaryal NFT only weakly and ghost tangles not at all. While an explanation for the different staining patterns of these antibodies is not readily apparent, there may be some cross-reactivity of the polyclonal antiserum with MAP-1, as shown in an immunoblot by Nukina and Ihara (ref. 55; Fig. 2).

NFT have been isolated here by two different methods: under denaturing conditions in boiling $NaDodSO_4$ and under

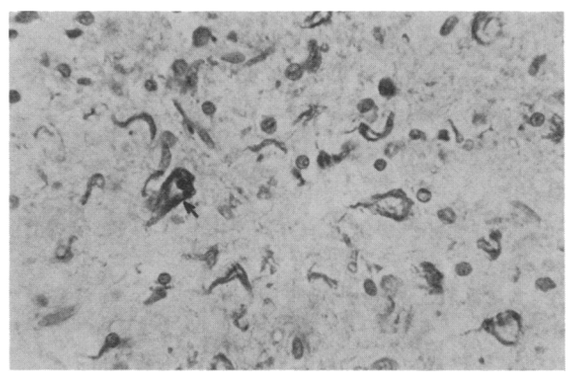

FIG. 8. NFT labeled with mAb 5F9 to MAP-2. Paraffin section of formalin-fixed Alzheimer disease CA1 region of hippocampus stained by the peroxidase-conjugated secondary-antibody method. Arrow indicates single intraneuronal tangle, which is stained more intensely than the numerous surrounding ghost tangles. (×225.)

physiologic conditions in Tris saline. After boiling in $NaDodSO_4$, the PHF in the tangles are retained (12), while many of the contaminants in the Tris saline NFT preparations, including virtually all normal neurofilaments and microtubules, are removed. Proteins non-covalently associated with the NFT would be expected to be solubilized and removed by $NaDodSO_4$ treatment. After $NaDodSO_4$ extraction, all of our mAb against MAP-2 failed to immunolabel NFT. The failure of 5F9 to stain the $NaDodSO_4$-extracted NFT may be either because the MAP-2 antigenic determinants were completely removed (and are therefore non-covalently bound) or because they were altered by heating in $NaDodSO_4$.

Evidence has begun to accumulate that MAP-2 may serve to cross-link microtubules with other cytoplasmic structures, including actin filaments (56–59), secretory granules (60), coated vesicles (61), and neurofilaments (36). In mature brain tissue, MAP-2 is immunocytochemically localized in the dendritic and perikaryal portions of neurons (27, 28). We have also shown that immunoblots of rabbit sciatic nerve and mouse optic nerve do not contain 5F9 immunoreactive bands despite the presence of the antigen in these species (unpublished data). Neurofilaments are also localized to neurons and tend to be enriched in axons rather than dendrites (8). The presence by immunocytochemical criteria of these two regionally polarized elements within the NFT suggests that the pathogenesis of the tangle involves, in part, a disruption of intraperikaryal traffic and changes in the normal asymmetrical sorting of cytoskeletal elements.

MAP-2 appears to become associated with 10-nm filaments under certain other cytopathological conditions—for example, disruption of the microtubular system by vinblastine (37). Aluminum-induced neurofilamentous bundles, however, do not contain MAP-2 immunoreactivity (unpublished data). Only the complete purification of PHF and subsequent elucidation of their primary amino acid sequence will allow a detailed analysis of the relationship of these fibers to normal cytoskeletal elements such as neurofilaments and MAP-2.

The authors wish to thank Dr. Miyuki Yamamoto for helpful discussions, Dr. Howard Weiner for the gift of NS1 cells, and Bethany Block for technical assistance. This work was supported in part by Grants NS 20110 and AG 01397 (D.J.S.) from the National Institutes of Health. K.S.K. is the recipient of Teacher–Investigator Award NS 00835 from the National Institute of Neurological and Communicative Disorders and Stroke.

1. Kidd, M. (1963) *Nature (London)* **197,** 192–193.
2. Terry, R. D. (1963) *J. Neuropathol. Exp. Neurol.* **22,** 629–642.
3. Wisniewski, H. M., Narang, H. K. & Terry, R. D. (1976) *J. Neurol. Sci.* **27,** 173–181.
4. Okamoto, K., Hirano, A., Yamaguchi, H. & Hirai, S. (1982) *Clin. Neurol.* **22,** 840–846.
5. Ghatak, N. R., Nochlin, D. & Hadfield, M. G. (1980) *Acta Neuropathol.* **52,** 73–76.
6. Shibayama, H. & Kitoh, J. (1978) *Acta Neuropathol.* **41,** 229–234.
7. Tellez-Nagel, I. & Wisniewski, H. M. (1973) *Arch. Neurol.* **29,** 324–327.
8. Peters, A., Palay, S. L. & de F Webster, H. (1976) *Fine Structure of the Nervous System* (Saunders, Philadelphia).
9. Yagishita, S., Itoh, Y., Nan, W. & Amano, N. (1981) *Acta Neuropathol.* **54,** 239–246.
10. Rewcastle, N. B. & Ball, J. J. (1968) *Neurology* **18,** 1205–1213.
11. Rewcastle, N. B. (1976) *Neuropathol. Appl. Neurobiol.* **2** (6), 490.
12. Selkoe, D. J., Ihara, Y. & Salazar, F. J. (1982) *Science* **215,** 1243–1245.
13. Anderton, B. H., Breinburg, D., Downes, M. J., Green, P. J., Tomlinson, B. E., Ulrich, J., Wood, J. M. & Kahn, J. (1982) *Nature (London)* **298,** 84–86.
14. Yen, S.-H. C., Gaskin, F. & Terry, R. D. (1981) *Am. J. Pathol.* **104,** 77–89.
15. Ihara, Y., Abraham, C. & Selkoe, D. J. (1983) *Nature (London)* **304,** 727–730.
16. Autilio-Gambetti, L., Gambetti, P. & Crane, R. C. (1983) in *Biological Aspects of Alzheimer's Disease*, Banbury Report 15, ed. Katzman, R. (Cold Spring Harbor Laboratory, Cold Spring Harbor, NY), pp. 117–124.
17. Rasool, C. G., Abraham, C., Anderton, B., Haugh, M., Kahn, J. & Selkoe, D. J. (1984) *Brain Res.*, in press.
18. Dahl, D., Selkoe, D. J., Pero, R. T. & Bignami, A. (1982) *J. Neurosci.* **2,** 113–119.
19. Ihara, Y., Nukina, N., Sugita, H. & Toyokura, Y. (1981) *Proc. Jpn. Acad.* **57,** 152–156.
20. Ishii, T., Haga, S. & Tukutake, S. (1979) *Acta Neuropathol.* **48,** 105–112.
21. Sloboda, R. D., Rudolph, S. A., Rosenbaum, J. L. & Greengard, P. (1975) *Proc. Natl. Acad. Sci. USA* **72,** 177–181.
22. Herzog, W. & Weber, K. (1978) *Eur. J. Biochem.* **92,** 1–8.
23. Vallee, R. B. (1980) *Proc. Natl. Acad. Sci. USA* **77,** 3205–3210.
24. Zingsheim, H. P., Herzog, W. & Weber, K. (1979) *Eur. J. Cell Biol.* **19,** 175–183.
25. Voter, W. A. & Erickson, H. P. (1982) *J. Ultrastruct. Res.* **80,** 374–382.
26. Kim, H., Binder, L. I. & Rosenbaum, J. L. (1979) *J. Cell Biol.* **80,** 266–276.
27. Matus, A., Bernhardt, R. & Hugh-Jones, T. (1981) *Proc. Natl. Acad. Sci. USA* **78,** 3010–3014.
28. Miller, P., Walter, V., Theurkauf, W. E., Vallee, R. B. & DeCamilli, P. (1982) *Proc. Natl. Acad. Sci. USA* **79,** 5562–5566.
29. Burton, P. R. & Fernandez, H. (1973) *J. Cell Sci.* **12,** 567–583.
30. Rice, R. V., Roslansky, P. F., Pascoe, N. & Houghton, S. M. (1980) *J. Ultrastruct. Res.* **71,** 303–319.
31. Tsukita, S. & Ishikawa, H. (1981) *Biochem. Res. (Tokyo)* **2,** 424–437.
32. Wuerker, R. B. & Palay, S. L. (1969) *Tissue Cell* **1,** 387–402.
33. Berkowitz, S. A., Katagiri, J., Binder, H. K. & Williams, R. C., Jr. (1977) *Biochemistry* **16,** 5610–5617.
34. Runge, M. S., Laue, T. M., Yphantis, D. A., Lifsics, M. R., Saito, A., Altin, M., Reinke, K. & Williams, R. C., Jr. (1981) *Proc. Natl. Acad. Sci. USA* **78,** 1431–1435.
35. Leterrier, J. F., Liem, R. K. H. & Shelanski, M. L. (1981) *J. Cell Biol.* **90,** 755–760.
36. Leterrier, J. F., Liem, R. K. H. & Shelanski, M. L. (1982) *J. Cell Biol.* **95,** 982–986.
37. Bloom, G. S. & Vallee, R. B. (1983) *J. Cell Biol.* **96,** 1523–1531.
38. Shelanski, M. L., Gaskin, F. & Cantor, C. R. (1973) *Proc. Natl. Acad. Sci. USA* **70,** 765–768.
39. Kennett, R. H. (1980) in *Monoclonal Antibodies*, eds. Kennett, R. H., McKearn, T. J. & Bechtol, K. B. (Plenum, New York), pp. 365–367.
40. Lambre, C. & Kasturi, K. N. (1979) *J. Immunol. Methods* **26,** 61–67.
41. Towbin, H., Staehelin, T. & Gordon, J. (1979) *Proc. Natl. Acad. Sci. USA* **76,** 4350–4354.
42. Vallee, R. B. (1982) *J. Cell Biol.* **92,** 435–442.
43. Laemmli, U. K. (1970) *Nature (London)* **227,** 680–685.
44. McKearn, T. J. (1980) in *Monoclonal Antibodies*, eds. Kennett, R. H., McKearn, T. J. & Bechtol, K. B. (Plenum, New York), pp. 374.
45. Sternberger, L. A. & Sternberger, N. H. (1983) *Proc. Natl. Acad. Sci. USA* **80,** 6126–6130.
46. Julien, J.-P. & Mushynski, W. E. (1982) *J. Biol. Chem.* **257,** 10467–10470.
47. Sternberger, L. A. (1979) *Immunocytochemistry* (Wiley, New York), 2nd Ed.
48. Cleveland, D. W., Fischer, S. G., Kirschner, M. W. & Laemmli, U. K. (1977) *J. Biol. Chem.* **252,** 1102–1106.
49. Escobar, M. I., Pimienta, H., Jacobson, M., Kosik, K. S., Crandall, J. E. & Caviness, V. S., Jr. (1984) *Soc. Neurosci. Abstr.* **10,** 428.
50. Jervis, G. A. (1948) *Am. J. Psychiatry* **105,** 192–196.
51. Burger, P. C. & Vogel, F. S. (1973) *Am. J. Pathol.* **73,** 457–476.
52. Ellis, W. G., McCullogh, J. R. & Corley, C. L. (1974) *Neurology* **24,** 101–106.
53. Grundke-Iqbal, I., Johnson, A. B., Wisniewski, H. M., Terry, R. D. & Iqbal, K. (1979) *Lancet* **i,** 578–580.
54. Johnson, A. B., Huang, M. & Fischberg, E. (1983) *J. Neuropathol. Exp. Neurol.* **42,** 335 (abstr.).
55. Nukina, N. & Ihara, Y. (1983) *Proc. Jpn. Acad.* **59,** 284–292.
56. Caceres, A., Payne, M. R., Binder, L. I. & Steward, O. (1983) *Proc. Natl. Acad. Sci. USA* **80,** 1738–1742.
57. Griffith, L. M. & Pollard, T. D. (1978) *J. Cell Biol.* **78,** 958–965.
58. Griffith, L. M. & Pollard, T. D. (1982) *J. Biol. Chem.* **257,** 9143–9151.
59. Sattilaro, R. F., LeCluyse, E. L. & Dentler, W. L. (1980) *J. Cell Biol.* **87,** 250a (abstr.).
60. Sherline, P., Lee, Y. C. & Jacobs, L. S. (1977) *J. Cell Biol.* **72,** 380–389.
61. Sattilaro, R. F., Dentler, W. L. & LeCluyse, E. L. (1981) *J. Cell Biol.* **90,** 467–473.